Phase separation in the nonequilibrium Verwey transition in magnetite

F. Randi,[1] I. Vergara,[2] F. Novelli,[3] M. Esposito,[1] M. Dell'Angela,[3] V. A. M. Brabers,[4] P. Metcalf,[5] R. Kukreja,[6,7] H. A. Dürr,[6] D. Fausti,[1,3,*] M. Grüninger,[2] and F. Parmigiani[1,3,8]

[1]*Department of Physics, Università degli Studi di Trieste, 34127 Trieste, Italy*

[2]*II. Physikalisches Institut, Universität zu Köln, 50937 Köln, Germany*

[3]*Sincrotrone Trieste SCpA, 34149 Basovizza, Italy*

[4]*Department of Physics, Eindhoven University of Technology, Eindhoven, The Netherlands*

[5]*Purdue University, School of Materials Engineering, West Lafayette, Indiana 47907, USA*

[6]*Stanford Institute for Materials and Energy Sciences, SLAC National Accelerator Laboratory, 2575 Sand Hill Road, Menlo Park, California 94025, USA*

[7]*Department of Materials Science and Engineering, Stanford University, 496 Lomita Mall, Stanford, California 94305, USA*

[8]*International Faculty, Universität zu Köln, 50937 Köln, Germany*

(Received 9 September 2015; revised manuscript received 1 December 2015; published 26 February 2016)

We present equilibrium and out-of-equilibrium studies of the Verwey transition in magnetite. In the equilibrium optical conductivity, we find a steplike change at the phase transition for photon energies below about 2 eV. The possibility of triggering a nonequilibrium transient metallic state in insulating magnetite by photo excitation was recently demonstrated by an x-ray study. Here we report a full characterization of the optical properties in the visible frequency range across the nonequilibrium phase transition. Our analysis of the spectral features is based on a detailed description of the equilibrium properties. The out-of-equilibrium optical data bear the initial electronic response associated to localized photoexcitation, the occurrence of phase separation, and the transition to a transient metallic phase for excitation density larger than a critical value. This allows us to identify the electronic nature of the transient state, to unveil the phase transition dynamics, and to study the consequences of phase separation on the reflectivity, suggesting a spectroscopic feature that may be generally linked to out-of-equilibrium phase separation.

DOI: 10.1103/PhysRevB.93.054305

I. INTRODUCTION

The Verwey phase transition, occurring at $T_V = 123$ K in magnetite (Fe_3O_4), is presumably the most studied metal-insulator transition in the large family of transition-metal oxides [1,2]. Detailed investigations of the structure revealed a stunning complexity [3–14]. Magnetite crystallizes with an inverse spinel structure [Fig. 1(a)], characterized by two different groups (A and B) of Fe ion sites. Group A is constituted by tetrahedrally coordinated Fe_A^{3+} sites with a $3d^5$ electronic configuration with spin $S = 5/2$. Group B, instead, is made of octahedrally coordinated sites formally occupied by Fe_B^{3+} ($3d^5$, $S = 5/2$) and Fe_B^{2+} ($3d^6$, $S = 2$) ions. At $T_c = 858$ K, ferrimagnetic order sets in with ferromagnetic coupling within the B sublattice and antiferromagnetic coupling between A and B sites such that the A sites carry minority spins $\downarrow$. The original picture of the Verwey transition at T_V involves a metallic high-temperature phase showing an equal number of Fe_B^{3+} and Fe_B^{2+} ions randomly distributed on the B sites opposed to an insulating low-temperature phase with a charge-ordered B sublattice [1], breaking the cubic symmetry in favor of a monoclinic one. Since the B ions form a frustrated pyrochlore lattice, the charge-order superstructure is rather involved, reflecting the competition between Coulomb interactions and the coupling to both the lattice and the orbital degrees of freedom [2,12]. Recently, it has been shown that the picture may need to be refined even further [3]. On top of the charge order, x-ray studies suggest that the single minority $\downarrow$ electron of an Fe_B^{2+} ion is delocalized over the neighboring Fe_B^{3+} sites, forming linear units of three Fe sites dubbed trimerons [3]. Such units are organized in a network where different trimerons are connected via angles of 60° or 120°. Since the Fe_B^{3+} sites are part of up to three different trimerons (sharing different t_{2g} orbitals [3]), the trimeron lattice tends to equalize the charges on the Fe_B sites and to increase the polarizability [15]. Furthermore, having the minority spin delocalized on different sites reduces the expected entropy associated to the Verwey transition to values closer to experimentally observed ones [3,16]. In this interpretation, it has been proposed [3] that the Verwey transition should be seen as a transition between a frozen trimeron network and a fluctuating network with shorter correlation length.

With x-ray pump-probe experiments [17] some of us investigated the quench of the insulating phase after the excitation with ultrashort pulses at 1.55 eV. In that work it has been found that the light-driven structural change occurs in a two-step process: After the initial local destruction of charge order triggered by photo excitation, phase separation occurs yielding metallic and residual insulating regions.

Optical measurements provide an efficient tool to unravel the changes of electronic and structural properties at the phase transition [18–21]. In magnetite, the equilibrium optical conductivity [22–24] shows a broad Drude peak in the metallic phase as well as its suppression at the metal-insulator transition. The optical properties at higher energies are dominated by two features peaking at about 0.6 eV and 2 eV. By comparison

*Corresponding author: daniele.fausti@elettra.eu

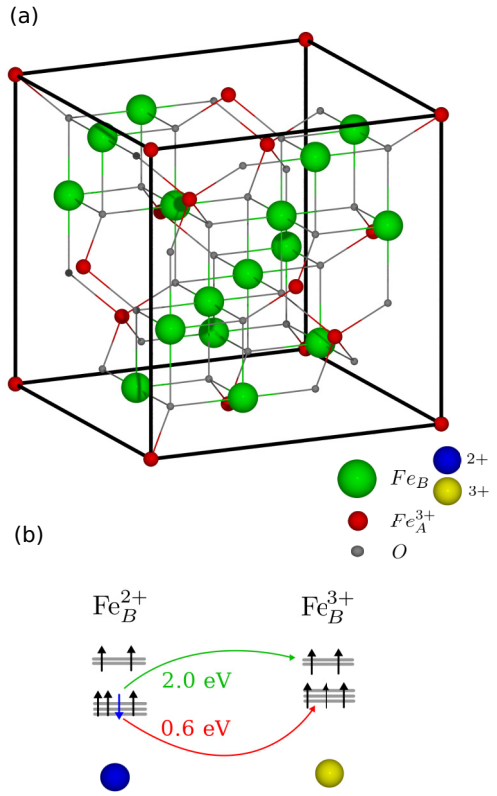

FIG. 1. (a) Inverse spinel high temperature structure of magnetite. (b) Sketch of the $Fe_B^{2+} \rightarrow Fe_B^{3+}$ transitions.

with LSDA+U results [25], these features were attributed to excitations of the minority $\downarrow$ electrons from the Fe_B^{2+} t_{2g} levels to the Fe_B^{3+} t_{2g} and e_g levels, respectively [see Fig. 1(b)]. However, alternative interpretations invoking the A sites were proposed for the feature at 2 eV [24,26]. Thus far, the behavior of these peaks at the Verwey transition has only been addressed at a qualitative level.

Here we report on detailed equilibrium and out-of-equilibrium measurements of the optical properties of magnetite in a broad spectral range. Ellipsometric data allow us to quantify the change of the equilibrium optical properties at the Verwey transition. The out-of-equilibrium measurements were performed under the same excitation conditions as used in combination with an x-ray probe in Ref. [17]. These measurements were performed at different temperatures to identify the analogies of the out-of-equilibrium insulator-to-metal transition with the thermodynamic one. While confirming the already described overall phase-transition dynamics, we discuss the consequences of out-of-equilibrium phase separation on the transient reflectivity. From these observations we propose a simple analysis to identify a spectroscopic feature that may be generally linked to out-of-equilibrium phase separation. Based on the analysis of the equilibrium data, we finally study the dynamics of the spectral features of the photoinduced transient state.

II. EXPERIMENTS

We performed pump-probe measurements on magnetite using 1.55 eV-centered 80 fs pulses as pumps and broadband pulses with spectral components extending from 1.7 eV to 2.5 eV as probes. The laser repetition rate was 250 kHz. More details of the setup have been described by Novelli *et al.* in Ref. [27]. No physical correction of the chirp of the broadband white light pulses was performed, but a post-processing correction of the chirp was applied to the data. Corrections to compensate the mismatch between the penetration depths at the pump photon energy and at the various probe photon energies (as described by Novelli *et al.* [28]) have been found not to be significant. The experiment was performed with the sample at 35 K, 80 K, and 140 K, the latter one being above the Verwey transition temperature. The out-of-equilibrium results reported here have been measured on two different samples, grown by the floating-zone technique in independent laboratories [17,29]. One of the samples was the same as used by de Jong *et al.* [17] in the time-resolved x-ray diffraction experiment. For the measurements of the equilibrium properties, we used a sample oriented in the [100] direction and polished to obtain an optically smooth surface. In the energy range from 0.75 eV to 3.5 eV, ellipsometric data were acquired with a rotating-analyzer ellipsometer (Woollam VASE) equipped with a retarder between polarizer and sample. The angle of incidence was 70°. The sample was mounted in a liquid-He flow cryostat with optical windows under UHV conditions ($< 10^{-9}$ mbar). For the analysis of the ellipsometric data, we assumed cubic symmetry and considered a surface roughness of 4 nm. The analysis directly yields the complex dielectric function $\varepsilon(\omega) = \varepsilon_1(\omega) + i\varepsilon_2(\omega)$, or, equivalently, the complex optical conductivity $\sigma(\omega) \propto i[\varepsilon(\omega) - 1]$.

III. RESULTS

A. Equilibrium optical properties

The solid lines in Fig. 2 depict $\sigma_1(\omega)$ and $\varepsilon_1(\omega)$ as determined from the ellipsometric data at selected temperatures. Overall, the data agree with previous results which were based on a Kramers-Kronig analysis of reflectivity data [22–24]. In $\sigma_1(\omega)$, strong absorption related to charge-transfer excitations from O_{2p} states to Fe_{3d} states sets in at about 2.5 eV, while the two absorption bands peaking at about 0.6 eV and 2 eV were attributed to excitations within the Fe_{3d} states [23–26]. With increasing temperature, the spectral weight of the 0.6 eV feature decreases, in agreement with the Kramers-Kronig results [23,24]. However, the literature data [23,24] do not address the precise behavior at the Verwey transition, and they disagree on the temperature dependence above 1.5 eV. This range is of particular importance for our pump-probe measurements with broadband probe pulses extending from 1.7 eV to 2.5 eV. Ellipsometry is a self-normalizing technique which directly yields the complex dielectric function without the need to invoke a Kramers-Kronig analysis. It therefore is particularly well suited to determine the precise temperature dependence of the optical properties [30–32]. The inset of Fig. 2 focuses on $\sigma_1(T)$ at three selected frequencies, revealing a steplike change of $\sigma_1(T)$ at T_V. This is a clear signature of the change of the electronic structure.

To provide a solid starting point for the analysis of the out-of-equilibrium optical data, we fitted the ellipsometric data using an oscillator model. The dashed lines in Fig. 2

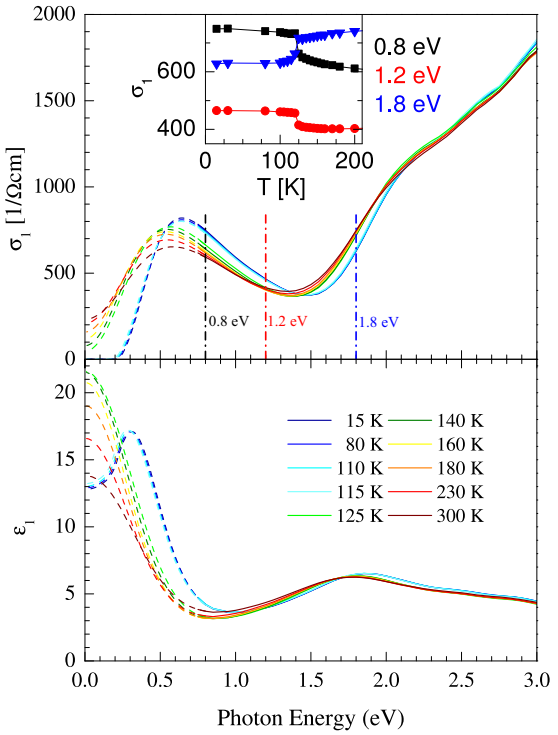

FIG. 2. Real parts $\sigma_1(\omega)$ and $\varepsilon_1(\omega)$ of the optical conductivity (top) and the dielectric function (bottom) as determined by ellipsometry (solid lines). Dashed lines show extrapolations based on fits of the ellipsometric data (see main text). The opening of a gap in σ_1 at low temperatures gives rise to the peak in ϵ_1 at about 0.3 eV. Inset: The temperature dependence of σ_1 at the three frequencies indicated in the main panel highlights steplike changes at T_V.

show the extension of the optical properties to lower photon energies provided by the model. We employed a Gaussian line shape for the features above 1.5 eV, while a Tauc-Lorentz profile was assumed for the absorption band peaking at about 0.6 eV since this band shows a gaplike feature in the insulating phase. In the metallic phase, the model includes a Drude peak describing free carriers, $\sigma_1^{\mathrm{Drude}} = \sigma_{\mathrm{DC}}/(1+\omega^2\tau^2)$. This Drude peak mainly contributes below the lower limit of our frequency range. Therefore, we fixed the two parameters σ_{DC} and τ of the Drude peak by using the measured DC resistivity and a temperature-independent value for the scattering rate $1/\tau$ which was adapted to describe the room-temperature data of Park and collaborators [24]. Consideration of the temperature dependence of this Drude peak via $\sigma_{\mathrm{DC}}(T)$ provides a more reliable determination of the properties of the prominent peak at 0.6 eV, of which our data covers only the high-energy side (see Supplemental Material [33]). Based on the assumption that this peak shows a Tauc-Lorentz profile we still may obtain a reasonable estimate of its properties as ellipsometry yields both $\varepsilon_1(\omega)$ and $\varepsilon_2(\omega)$, providing a strong constraint for the fits. This is corroborated by the reasonable agreement between our fits and the low-energy results for ε_1 of Ref. [22] and for $\sigma_1(\omega)$ of Refs. [23] and [24] concerning, e.g., the peak frequency of about 0.6 eV, the peak height, and the size of the gap Δ in the insulating phase. Our fits yields $\Delta = 0.2$ eV at 15 K, which coincides with the value reported by Gasparov *et al.* [23], while Park *et al.* [24] find 0.14 eV. Even though the quantitative

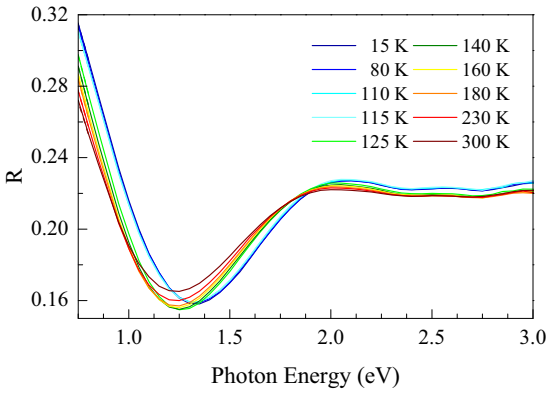

FIG. 3. Equilibrium reflectivity derived from the ellipsometric results plotted in Fig. 2.

results for the low-energy oscillator have to be taken with some care, our model provides an excellent basis for the analysis of the out-of-equilibrium data measured between 1.7 eV and 2.5 eV, well within the range covered by our ellipsometric data. The corresponding equilibrium reflectivity spectra are plotted in Fig. 3 at selected temperatures. The fit results fully reproduce the data depicted in Fig. 2. Note that the steplike changes of $\sigma_1(T)$ at T_V do not necessarily correspond to a discontinuity in the spectral weight of the oscillators, which, as shown in Fig. 4, display a continuous temperature dependence.

The spectral weight denotes the integral of a given feature in $\sigma_1(\omega)$. The temperature dependence of the spectral weights of the different contributions to the oscillator model are depicted in Fig. 4. Following the gradual change of the DC resistivity, the Drude peak loses spectral weight upon cooling and vanishes at the metal-insulator transition at T_V. This change of spectral weight is roughly compensated by the Tauc-Lorentz oscillator at 0.6 eV, the sum of the spectral weights of the two features is nearly independent of temperature (see open symbols). This is consistent with the results of Gasparov *et al.* [23], who reported that the spectral weight is roughly independent of T below about 0.8 eV. This agreement further supports the reliability of our model. The gradual change of both the Drude peak and the Tauc-Lorentz oscillator extends to temperatures far above T_V, which was attributed to short-range charge order [24]. Note that this gradual change can also be

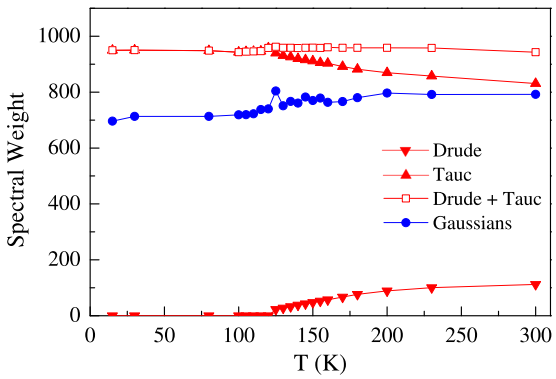

FIG. 4. Temperature dependence of the spectral weights of different oscillators used in the model (see dashed lines in Fig. 2).

observed in the ellipsometry result for $\sigma_1(T)$ (see inset of Fig. 2), i.e., independent of any oscillator model. Qualitatively, the T dependence in the visible range (blue symbols in Fig. 4) is similar to that of the Tauc-Lorentz oscillator, albeit with the opposite sign.

B. Out-of-equilibrium optical properties

Our out-of-equilibrium data can be separated into two classes. The data measured at 35 K and 80 K ($T < T_V$) show similar behavior, which we will argue to be the out-of-equilibrium equivalent of the Verwey transition. The data measured at 140 K ($T > T_V$), instead, do not show the distinctive features displayed below T_V, linked to the photoinduced phase transition. Since the results at 35 K and 80 K are almost completely equivalent, for the sake of clarity we will describe and discuss explicitly only the results at 35 K, underlining where the differences with the data at 80 K arise and how these differences support the picture drawn for 35 K (see the Supplemental Material [33] for plots of the data at 80 K).

The results at 35 K allow us to identify three regimes of pump fluence F in which the relative variation of the reflectivity $[\frac{\Delta R}{R}(t,h\nu)]$ behaves qualitatively different. The only difference with the results at 80 K are the pump fluences delimiting these intervals, which are shifted to lower values for higher temperature. In Fig. 5 we plot three data sets for selected fluences, each of them representative of one of the three regimes. In Fig. 6 instead, we plot $\frac{1}{F}\frac{\Delta R}{R}(t)$ at $h\nu = 1.74$ eV for all the fluences F.

Below a pump fluence of $F_1 = 2.7\,\mathrm{mJ\,cm^{-2}}$, the relative variation of the reflectivity $\frac{\Delta R}{R}(t,h\nu)$ behaves as shown in Fig. 5(a). In this regime, which in the following we will call *low fluence*, the response has two distinctive features. First of all, after a very fast increase at pump-probe delay $t = 0$ at low probing energies around 1.8 eV, $\frac{\Delta R}{R}$ decays exponentially with a characteristic time scale of 0.9 ps to a nonzero thermal plateau [see inset of Fig. 5(a) and Fig. 6]. The second feature is that $\frac{\Delta R}{R}$ scales linearly with the fluence, as can be seen in Fig. 6. This behavior is typical of the creation of excitations, whose density scales linearly with the pump fluence. The excitations then decay bringing the system to a thermalized state with a temperature different from the initial one. The lifetime of this transient state is determined by the thermal conductivity of the system.

In the *intermediate fluence* regime between F_1 and $F_2 = 5.1\,\mathrm{mJ\,cm^{-2}}$, a behavior like the one plotted in Fig. 5(b) becomes visible. Again, we can identify two characteristic features. First, the excitation is followed by two distinct dynamics. After quickly decaying for a very short time (<1 ps), the response grows again on a slower time scale τ_2 [see inset of Fig. 5(b)]. This happens more pronouncedly on the low-energy side of the probed range. Second, while the amplitude of the initial peak ($t \simeq 0.2$ ps) still scales linearly with the fluence (as in the low fluence regime), the amplitude of the long-time dynamics does not and its characteristic timescale is not constant with the fluence (see Fig. 6). In particular, the latter becomes faster as the fluence increases. From these considerations we can say that the creation of a sufficient number of excitations in the system triggers a new dynamical

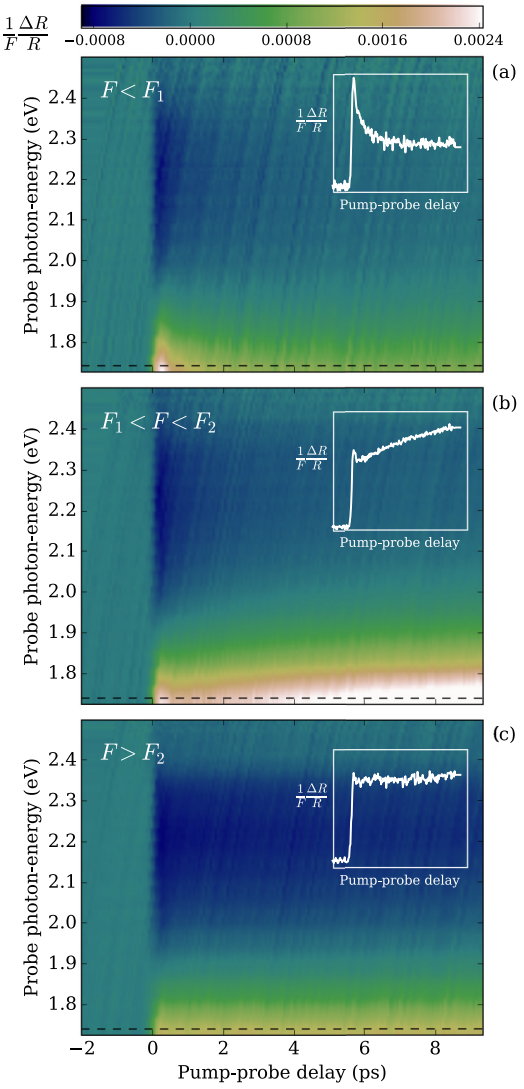

FIG. 5. Normalized relative variation of the reflectivity $\frac{1}{F}\frac{\Delta R}{R}(h\nu,t)$ at 35 K for pump fluences F of (a) $0.5\,\mathrm{mJ\,cm^{-2}}$, (b) $4.6\,\mathrm{mJ\,cm^{-2}}$, and (c) $7.1\,\mathrm{mJ\,cm^{-2}}$, characteristic of the three regimes of low, intermediate, and high fluence. Insets: $\frac{\Delta R}{R}(t)$ at 1.74 eV for the respective fluences. Dashed lines: photon-energy corresponding to the insets.

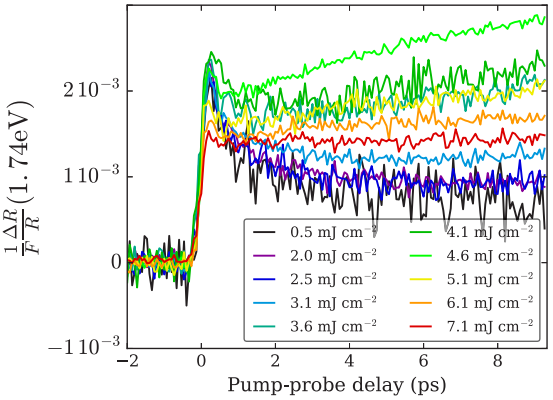

FIG. 6. Normalized relative variation of the reflectivity $\frac{1}{F}\frac{\Delta R}{R}(h\nu = 1.74\ \mathrm{eV},t)$ at 35 K for all the available pump fluences.

response, evolving on a larger time scale than the decay of the excitations.

In the *high fluence* regime, starting from F_2, $\frac{\Delta R}{R}$ progressively loses the mentioned features, as shown in Fig. 6, up to the point that for the highest measured fluence (7.1 mJ cm^{-2}) it behaves as a switch on the low-energy side of the spectrum, as shown in Figs. 5(c) and 6. In this regime, $\frac{\Delta R}{R}$ is almost independent of the fluence. Moreover, apart from a small relaxation on the high-energy side of the spectrum, $\frac{\Delta R}{R}$ displays a steplike behavior at $t = 0$ and does not evolve anymore for times at least longer than 10 ps.

IV. DISCUSSION

By means of time-resolved x-ray diffraction, de Jong *et al.* [17] have shown that holes in the charge-ordered lattice, purportedly the trimeronic lattice [3], are produced upon excitation by the pump pulse. If the pump fluence is lower than F_1, the lattice thermalizes to a higher temperature but retains the global symmetry of the low-temperature charge-ordered phase (*low fluence* regime). If the fluence exceeds F_1, nucleation of volumes with the symmetry of the high-temperature phase is triggered. This leads to phase separation, i.e., coexistence of uncorrelated charge-ordered regions and metallic ones (*intermediate fluence* regime). Our time-resolved spectroscopic data confirm this scenario. Moreover, we also explored higher fluences ($F > F_2$), where the dynamics is different.

Our discussion will proceed as follows. First, we will discuss the intermediate fluence regime and we will show that the spectral feature of the long-time response corresponds to the nucleation of the high-temperature phase. We will afterwards identify what could be general consequences of phase separation on the separability of the out-of-equilibrium reflectivity of a system. We will then show that in the high fluence regime the system is, instead, immediately (i.e., on a timescale smaller than our experimental resolution) and homogeneously brought to the high-temperature phase, and the nucleation process can no longer be observed in the out-of-equilibrium optical properties. Residual localized charge order is still present in the system, but the insulating region is progressively reduced as the fluence increases. This scenario emerges from the comparison of the out-of-equilibrium with the equilibrium measurements and from the study of the separability of the variation of the reflectivity as a function of time and probe photon energy.

The results obtained at 140 K confirm that our observations can be ascribed to a photoinduced phase transition. Above the Verwey transition temperature and for the measured fluences the response is linear, and there is no evidence for a photoinduced phase transition. In the following we will use this substantial difference to benchmark part of the proposed analysis.

A. Out-of-equilibrium phase transition and its relation to equilibrium

In this section we first present plots of quantities parameterizing both the fast and the long-time response of the system and identify the critical fluences to initiate (F_1) and saturate

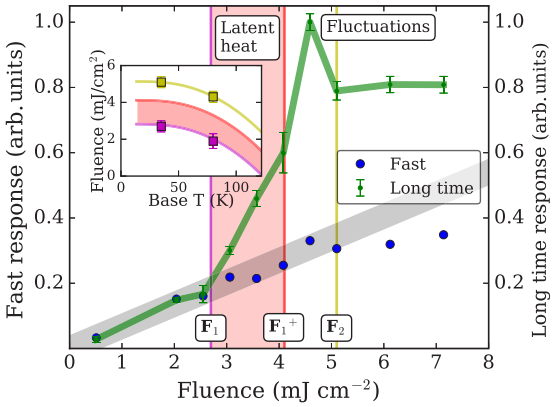

FIG. 7. "Fast response" (blue circles): $\frac{\Delta R}{R}$ at 1.74 eV photon energy and 0.2 ps pump-probe delay. "Long-time response" (green dots): $\frac{\Delta R}{R}$ at 1.74 eV photon energy and 8 ps pump-probe delay. Inset: The squares are the characteristic fluences extracted from the out-of-equilibrium data as a function of the sample's temperature, corresponding to: onset of the nonlinear response (magenta) and saturation of the nonlinear response (yellow). The lines represent equivalent fluences calculated from thermodynamic data needed to: reach T_V^- (magenta), reach T_V^+ (red), reach 140 K (yellow). The red shaded area corresponds to fluences bringing the sample to T_V^- and supplying part of the latent heat. The vertical lines and the vertical shaded area in the main figure mimic the inset.

(F_2) the out-of-equilibrium phase transition. Subsequently we relate the fluences F_1 and F_2 with effective temperatures of the system after the excitation and compare them with temperatures relevant in the equilibrium thermodynamics and optical properties.

In Fig. 7, we plot $\frac{\Delta R}{R}$ as a function of fluence F at a pump-probe delay of 0.2 ps and at 1.74 eV, a representative photon-energy (blue circles). As mentioned above, this quantity scales linearly with the fluence below F_2 (5.1 mJ cm^{-2}). Above F_2 it saturates, in correspondence with the switchinglike behavior [see Figs. 5(c) and 6]. Second, in the same figure we plot $\frac{\Delta R}{R}$ at 8 ps, again at 1.74 eV as a function of fluence (green dots). In this case there are two characteristic fluences. Below F_1 the system quickly relaxes to a thermal state and $\frac{\Delta R}{R}$(1.74 eV) at 8 ps follows the same linear behavior as it does at 0.2 ps, as shown in Fig. 6. Between F_1 and F_2 the long-time response departs from the linear scaling of the low fluence regime, i.e., it displays the nonlinear slow behavior [see Figs. 5(b) and 6]. Finally, above F_2 the saturation of $\frac{\Delta R}{R}$, occurring when the switchinglike behavior is reached, is also present in this plot [Figs. 5(b) and 6].

These fluences correspond to characteristic temperatures relevant in equilibrium thermodynamic and optical data. In fact, assuming a thermal state of the system, we can calculate its effective temperature after the delivery of energy by a single pump pulse. This can be done comparing the energy absorbed by the excited volume of the sample from each pump pulse and the integral of the equilibrium specific heat of magnetite. In particular the excited volume is estimated under simple assumptions (for details of the calculation, see the Supplemental Material [33]). A pump pulse with F_1 delivers an amount of energy which heats the system from its base temperature of 35 K to T_V^-, i.e., right to the Verwey transition

temperature without supplying any latent heat. Above F_1, the surplus of energy triggers the phase transition and the dynamic nucleation of the metallic phase, as inferred from the x-ray diffraction data by de Jong *et al.* [17]. The system is brought to T_V^+, i.e., supplied with the full latent heat, by $F_1^+ = 4.1\,\mathrm{mJ\,cm^{-2}}$. We will discuss the role of this fluence in the next section, showing how the qualitative change of behavior which becomes manifest above F_2 already starts for $F > F_1^+$. A pump fluence of F_2 heats the system to an effective temperature of about 140 K. At this temperature the fluctuations towards charge ordering are still clearly visible in the equilibrium optical properties (see the inset of Fig. 2). We argue that increasing the fluence above F_2, the variation of the electronic properties upon excitation goes towards being a sudden process, and the nucleation process is no longer observable in the out-of-equilibrium optical properties. Above F_2, $\frac{\Delta R}{R}$ in fact progressively loses all the characteristic features of the lower fluences. We will further support this hypothesis in the following sections.

In the inset of Fig. 7, we plot the calculated fluences corresponding to the mentioned final temperatures (T_V^-, T_V^+, and 140 K) for initial temperatures between 15 K and T_V^- (lines). Moreover we also plot the characteristic fluences (F_1 and F_2) measured at 35 and 80 K (squares). As shown, the characteristic fluences at 80 K are lower than the ones at 35 K, because at 80 K less energy is needed to bring the sample to the transition temperature.

B. Nucleation of the metallic phase, out-of-equilibrium phase separation, and nonseparability of the response

In this section we will present an analysis suggesting that the response of magnetite is homogeneous over the illuminated sample for base temperatures below T_V in the low and high fluence regimes, while the dynamics triggered in the intermediate regime involves phase separation. We will proceed as follows. At first, we will show that in the intermediate fluence regime $\frac{\Delta R}{R}(h\nu,t)$ is nonseparable, i.e., it can, and must, be written as the sum of two different spectral features evolving in time in two different ways. Subsequently, the two observed spectrotemporal features will be linked to: (i) the production and relaxation of excitations in the charge-ordered phase and (ii) the nucleation of the high-temperature phase.

As a visual reference for what follows, we plot $\frac{1}{F}\frac{\Delta R}{R}$ at 1.74 eV in Fig. 8(a) for representative fluences of the three regimes. As already mentioned, $\frac{\Delta R}{R}$ scales linearly with the fluence at all times below F_1, while between F_1 and F_2 only the fast response does. We can therefore isolate the nonlinear term ($\frac{\Delta R'}{R}$) between F_1 and F_2 by calculating

$$\frac{1}{F}\frac{\Delta R'}{R} = \frac{1}{F}\frac{\Delta R}{R} - \frac{1}{F_0}\frac{\Delta R}{R}\bigg|_0, \tag{1}$$

where F_0 is the lowest fluence that we have used experimentally.

In the intermediate fluence regime, the subtraction gives the result shown in Figs. 8(b) and 8(c) for $F = 4.6\,\mathrm{mJ\,cm^{-2}}$. There are three important features which can be noticed. First, $\frac{\Delta R'}{R}$ at $t = 0.2$ ps is 0 for all probe-photon energies. The nonlinear

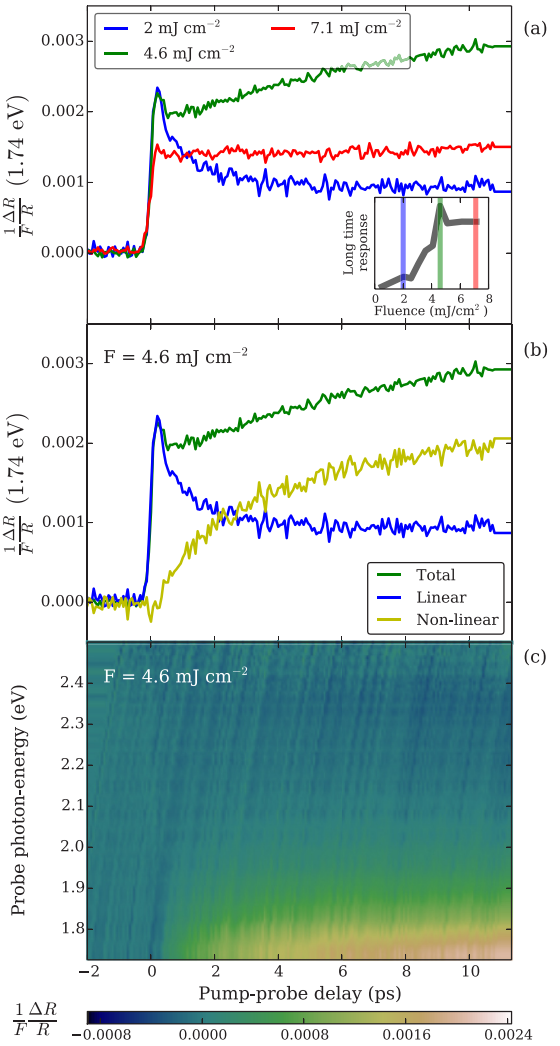

FIG. 8. (a) $\frac{1}{F}\frac{\Delta R}{R}(t)$ at 1.74 eV for $2.0\,\mathrm{mJ\,cm^{-2}}$ (blue), $4.6\,\mathrm{mJ\,cm^{-2}}$ (green), $7.1\,\mathrm{mJ\,cm^{-2}}$ (red) pump fluences. Inset: visual reference to Fig. 7. (b) Green: as in (a). Blue (yellow): linear (nonlinear) term of $\frac{1}{F}\frac{\Delta R}{R}$ for $F = 4.6\,\mathrm{mJ\,cm^{-2}}$ at 1.74 eV photon-energy. (c) $\frac{1}{F}\frac{\Delta R'}{R}(h\nu,t)$ for $F = 4.6\,\mathrm{mJ\,cm^{-2}}$.

$\frac{\Delta R'}{R}$ is therefore characterized by a purely slow dynamics. Second, the timescales τ_2 of the nonlinear/slow response match the ones obtained by de Jong *et al.* [17] for the emergence of regions with the high-temperature symmetry in the same excitation conditions (see Supplemental Material [33]). This demonstrates that the decomposition is physically meaningful, which is remarkable from a spectroscopic point of view since it entails the third important property: The total reflectivity is given by the *sum* of two terms which by themselves have physical meaning. The additivity of the response is consistent with the scenario in which the total reflectivity of the sample is given by the sum of the reflectivities of distinct regions sufficiently defined to have their own optical properties. In the case of out-of-equilibrium magnetite, these regions are the charge-ordered insulating phase and the nucleating metallic patches. Moreover, τ_2 decreases with increasing fluence. In fact, higher densities of excitations in the charge ordered lattice

produce smaller times for the nucleation, eventually leading to a percolative path in the high temperature phase.

The analysis proposed above is limited to fluences between F_1 and F_2 (and trivially below F_1). Above F_2, $\frac{\Delta R}{R}$ shows a resolution-limited switchlike behavior and the subtraction described in Eq. (1) is no longer applicable. We stress that the additivity of the spectroscopic response applies solely to the intermediate fluence regime, in which out-of-equilibrium x-ray diffraction showed the occurrence of phase separation in the system [17]. Moreover, as discussed in the previous section, there is a straightforward correspondence between the intermediate regime and the supply of latent heat in equilibrium thermodynamics, a situation in which it is natural to expect phase separation.

In order to check that this result is not just a consequence of a biased physical picture, we performed the singular value decomposition (see Supplemental Material [33]) on the matrices $[\frac{\Delta R}{R}]_{h\nu,t}$, where the row and column indices are the probe-photon energy and the pump-probe delay, respectively. We stress that the singular value decomposition algorithm is derived imposing constraints on the general problem of the factorization of a matrix. In particular, the sets of left and right singular vectors are required to be orthonormal bases. These constraints may lead to singular spectrotemporal features (left and right singular vectors) which are not suitable for a physical interpretation. In spite of this limitation which is due to the "unphysical" mathematical constraints, it is important to note that if the number of relevant [34] singular values is larger than 1, the matrix is not separable, i.e., it cannot be factorized as a single product of a spectral feature with one single temporal evolution for all the photon energies. This result is independent from the constraints.

In our data, the relevant singular values are at most two (see Supplemental Material [33], Fig. S2). In Fig. 9 we plot the ratio of the second largest singular value and the largest one (from both, the noise level was subtracted). A large ratio provides evidence for the existence of two different spectrotemporal features, in which case the matrix $[\frac{\Delta R}{R}]_{h\nu,t}$ is not separable (i.e., not factorizable) in $(h\nu,t)$ space. Therefore, we refer to this ratio as "nonseparability" in $(h\nu,t)$ space.

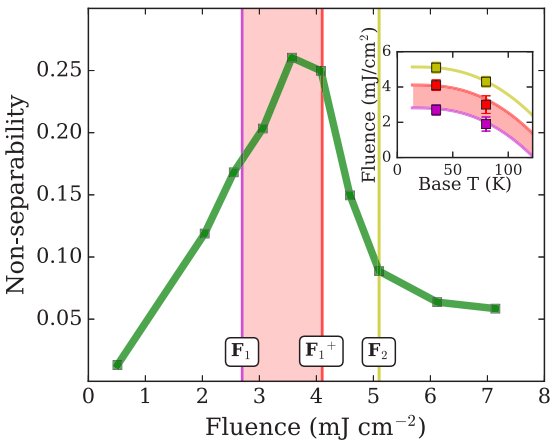

FIG. 9. Ratio of the second largest and largest singular values (from both, the noise level was subtracted), as a function of fluence. Inset: same inset as in Fig. 7, with the addition of the fluences at which the "nonseparability" starts to decrease (red squares), as measured at 35 and 80 K. These match the calculated equivalent fluences needed to deliver the full latent heat to the sample (red line).

As depicted in Fig. 9, $\frac{\Delta R}{R}$ is the furthest from being separable in the intermediate region. Starting from zero, as the fluence increases, $\frac{\Delta R}{R}$ ceases to be separable and the relevance of the additional spectrotemporal feature increases, until the pump pulse is intense enough to deliver all the latent heat. Up to this point the pump does not deliver the energy to bring the whole illuminated sample to the high-temperature phase and the nucleation of holes in the charge ordered lattice is needed to bring small islands to the high-temperature phase. Beyond that fluence ($F_1^+ = 4.1\,\mathrm{mJ\,cm^{-2}}$ as defined in the previous section), the "nonseparability" begins to decrease and the out-of-equilibrium system becomes approximately homogeneous again for $F > F_2$. In the high fluence regime, in fact, $\frac{\Delta R}{R}$ can be expressed almost as a single spectrotemporal feature. It must be pointed out, however, that the constraints on the shape of the singular vectors affect also the exact quantitative relation between the singular values and the weights of the physical components. Therefore, the edge at the threshold fluence in Fig. 9 does not necessarily resemble the physical edge in Fig. 7 (for more details, see the Supplemental Material [33]).

To benchmark this procedure, we performed the singular value decomposition on the data obtained at 140 K, where we do not expect phase separation to occur, i.e., where we expect the sample to be homogeneous. The results show that $\frac{\Delta R}{R}|_{140\,\mathrm{K}}$ is exactly separable (factorizable) as a single spectral feature evolving in time for all the pump fluences explored, supporting the outlined picture and analysis. The convergence of all these indications allow us to conjecture that the nonseparability of $\frac{\Delta R}{R}(t,h\nu)$ may be a general condition for the identification of phase separation in out-of-equilibrium systems.

C. Equilibrium optical properties across the phase transition

We now discuss the assignment of the features observed in the equilibrium optical properties to the excitations in magnetite. For this purpose it is useful to consider the LSDA+U results of Leonov and collaborators [25]. Charge-transfer excitations from O_{2p} states to Fe_{3d} states typically show much more spectral weight than transitions between Fe_{3d} states. These strong charge-transfer excitations set in at about 2.5 eV [24,25]. Accordingly, the features at 0.6 eV and 2 eV can be attributed to excitations between Fe_{3d} states. Since there are A and B sites as well as Fe^{2+} ($3d^6$) and Fe^{3+} ($3d^5$) ions, there is a multitude of possible excitations. However, the $3d^5$ configuration with only parallel spins ($S = 5/2$) is very stable, hence intersite excitations of the type $3d_i^5 3d_j^5 \rightarrow 3d_i^4 3d_j^6$ in which an electron is hopping from site i to site j are typically observed above 3 eV [35,36]. Therefore, it is reasonable to assume that the two features at 0.6 eV and 2 eV correspond to $3d_i^6 3d_j^5 \rightarrow 3d_i^5 3d_j^6$ excitations.

Among the occupied states, the minority $\downarrow$ electron within the t_{2g} level of an Fe_B^{2+} site is closest to the Fermi level E_F, while the lowest unoccupied states were identified as the empty t_{2g} $\downarrow$ states of Fe_B^{3+} sites [25]. The peak at 0.6 eV can thus be attributed to an intersite excitation involving these two states [23–25]. This excitation gains spectral weight with

increasing charge disproportionation between neighboring Fe_B sites, i.e., upon cooling towards the Verwey transition to the charge-ordered state.

In Fe_3O_4, neighboring Fe_B sites are connected via 90° Fe-O-Fe bonds, which allow not only for intersite $t_{2g} \rightarrow t_{2g}$ hopping relevant for the excitation at 0.6 eV but also for intersite $t_{2g} \rightarrow e_g$ hopping (see, e.g., Ref. [2]). According to LSDA+U results [25], the intersite excitation of the minority $\downarrow$ t_{2g} electron from an Fe_B^{2+} site to the empty e_g $\downarrow$ states on an Fe_B^{3+} site is located at about 2 eV. The temperature dependence of the spectral weight of this excitation is more subtle. At first sight, one may expect the same temperature dependence as for the 0.6 eV feature, since in both excitations the minority $\downarrow$ electron from an Fe_B^{2+} site is hopping to a $\downarrow$ state on an Fe_B^{3+} site. This disagrees with our experimental result which shows the opposite temperature dependence for the two features at 0.6 eV and 2 eV, see Fig. 4. However, Leonov *et al.* [25] find that charge order is strongly screened by a change of covalency, i.e., below T_V Fe_B^{3+} sites show an *enhanced* occupation of the e_g $\downarrow$ levels arising from hybridization with O_{2p} states. Accordingly, the spectral weight for excitations into the e_g levels is *reduced* upon entering the charge-ordered state.

Due to the Pauli principle, the minority $\downarrow$ electron from an Fe_B site may not hop to an Fe_A site where all $\downarrow$ states within the 3d shell are occupied. Alternatively, it has been proposed [24,26] that the peak at 2 eV corresponds to excitations of a majority $\uparrow$ electron from a Fe_B^{2+} ($3d^6$) site to an empty e_g level at an Fe_A^{3+} site. According to LSDA+U results, this excitation is expected at a slightly larger energy than the one described above [25].

D. Spectral response of the phase transition

On the basis of the above discussion we bring our final evidence to support the proposed discussion of the photoinduced phase transition. We present the spectral analysis of the features appearing in $\frac{\Delta R}{R}$. It will allow us to show that they are indeed associated to the charge-ordered and the charge-disordered phases. To do this we will resort to fits of $\frac{\Delta R}{R}$ by changing parameters of the oscillator model of the equilibrium optical properties. From such fits we can obtain two kinds of information. The first is the minimal set of free parameters (or oscillators) needed to account for the observed variation of the reflectivity. The second kind of information is the temporal evolution of the free parameters. We will restrict our discussion to the evolution of the spectral weights of the oscillators which is the most reliable outcome of the fits.

In the low fluence regime ($F < F_1$), the $\frac{\Delta R}{R}$ in the measured spectral range can be fully described by a variation of the oscillator in the infrared (0.6 eV), arising from $Fe_B^{2+}t_{2g} \rightarrow Fe_B^{3+}t_{2g}$ transitions, and the oscillator centered at 2 eV corresponding to the $Fe_B^{2+}t_{2g} \rightarrow Fe_B^{3+}e_g$ transitions [25]. The fit is shown in Fig. 10(a) for 0.2 ps pump-probe delay (magenta line). Modifications of the charge-transfer excitations between O_{2p} and Fe_{3d} are, instead, not needed to describe the observed dynamical response. In Fig. 10(b) we plot the temporal evolution of the spectral weights of the involved oscillators (for more details about the fitting procedure, see the Supplemental Material [33]). As excitations are created in the system at $t = 0$, the spectral weight of the $Fe_B^{2+}t_{2g} \rightarrow Fe_B^{3+}t_{2g}$ (0.6 eV) transition

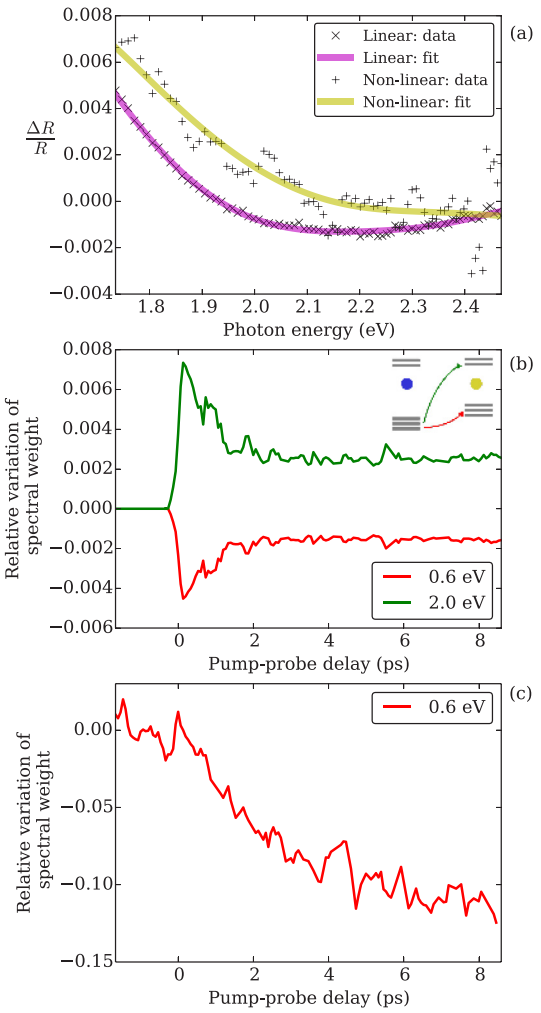

FIG. 10. (a) Linear and nonlinear terms in $\frac{\Delta R}{R}$ at 0.2 ps and 8.0 ps, respectively, and their fits. (b) Variation of the spectral weight as a function of pump-probe delay of the 0.6 (red) and 2.0 (green) oscillators as resulting from the fit of the linear/low-fluence $\frac{\Delta R}{R}$. Inset: sketch of the involved transitions. (c) Variation of the spectral weight of the 0.6 eV oscillator from the fit of the nonlinear term of $\frac{\Delta R}{R}$.

decreases while the one of the $Fe_B^{2+}t_{2g} \rightarrow Fe_B^{3+}e_g$ transition (2 eV) increases, then relaxing to a thermal plateau. The opposite signs of these variations are consistent with the opposite temperature behavior of the two features observed in the equilibrium data, see Fig. 4. On one side the partial destruction of the charge order reduces the spectral weight of the 0.6 eV oscillator, while on the other the dehybridization of the $Fe_B^{3+}e_g$ and O_{2p} states increases the weight of the 2 eV oscillator.

We then analyze the nonlinear term $\frac{\Delta R'}{R}$ arising in the intermediate fluence regime, linked to the nucleating phase. As shown in Fig. 10(a), it can be accounted for simply by a change of the $Fe_B^{2+}t_{2g} \rightarrow Fe_B^{3+}t_{2g}$ transition (0.6 eV oscillator). Its spectral weight decreases with the timescale characteristic of the slow dynamics [as shown in Fig. 10(c)], consistently with the picture in which the nucleating phase is the charge-disordered one. These results suggest that the hybridization of $Fe_B^{3+}e_g$ and O_{2p} states is not involved in the

nucleation process but is exclusively linked to the increase of the temperature of the system.

V. CONCLUSIONS

We reported measurements of both equilibrium and out-of-equilibrium optical properties of magnetite on a broad spectral range and at different temperatures across the Verwey insulator-to-metal phase transition. The equilibrium optical properties show a steplike behavior at the transition between the charge-ordered and charge-disordered phases. Our measurements allowed us also to determine the behavior of the spectroscopic features as a function of temperature. The most important ones in this discussion are the intersite transitions of minority spins $\downarrow$ from the $Fe_B^{2+}t_{2g}$ levels to the t_{2g} and e_g levels of Fe_B^{3+} atoms. As expected, the spectral weight of the $Fe_B^{2+}t_{2g} \rightarrow Fe_B^{3+}t_{2g}$ oscillator grows upon cooling, i.e., upon increasing charge disproportionation. The temperature dependence of the spectral weight of the $Fe_B^{2+}t_{2g} \rightarrow Fe_B^{3+}e_g$ oscillator is instead opposite. It decreases upon cooling as charge ordering enhances the hybridization of Fe_B^{3+} e_g with O_{2p} orbitals and hence gives rise to an increased minority spin $\downarrow$ occupation of the $Fe_B^{3+}e_g$ states.

The out-of-equilibrium data allowed us to draw various conclusions on the observed dynamics. Its excitation fluence dependence reveals that the photoexcitation process can trigger the out-of-equilibrium transition analogous of the Verwey phase transition, as already reported by de Jong *et al.* [17]. Below a certain threshold fluence ($F < F_1$, *low fluence* regime), the dynamical response we observe is the one associated with a warmer charge-ordered lattice, homogeneous over the sample. With larger fluences ($F_1 < F < F_2$, *intermediate fluence* regime), regions of the high temperature phase can nucleate, eventually leading to isolated remnants of the charge-ordered lattice [17]. This picture of the nature of the nucleating phase is supported by the spectral analysis of our out-of-equilibrium data. Moreover, the latter also contain indications about the phase separation occurring in the sample. In fact, in the intermediate fluence regime $[\frac{\Delta R}{R}]_{hv,t}$ is not a separable matrix, i.e., it cannot be expressed as a single spectral feature evolving in time. This points to the fact that the observed response is the sum of the responses of distinct regions. Finally, we have shown that above a further threshold fluence ($F > F_2$, *high fluence* regime), the transition to the high temperature phase is homogeneous over the sample and nucleation is not observed in the electronic properties as it is in the intermediate fluence regime. The mentioned characteristic fluences are surprisingly linked within the experimental error to the equilibrium thermodynamics of magnetite and in particular to the delivery of latent heat to the sample. This suggests that the photoexcitation with 1.5 eV photons acts as a sudden heating. Furthermore, the light-induced phase can be qualitatively linked to the equilibrium high temperature phase studying its spectral fingerprint in the visible, which maps the local charge order. We stress that our visible probe cannot measure the Drude response associated with a metallic behavior. Further measurements addressing the low energy optical properties are therefore necessary to ascertain the full correspondence between the light-induced phase and the equilibrium high temperature metallic one.

Our results about the phase separation in the system may have a general relevance beyond the particular case study of magnetite. Although the details as the lattice order and the timescales involved could be different, the behavior we discussed in this paper may be valid in general for photoexcited out-of-equilibrium systems displaying a first order phase transition. Furthermore, the picture emerging from this paper suggests also that a nonseparable out-of-equilibrium reflectivity may be a general fingerprint of out-of-equilibrium phase separation and may represent a straightforward way to identify phase separation in other out-of-equilibrium experiments. Further studies on different systems are needed to assess the natural occurrence of phase separation in light driven first order phase transformations.

ACKNOWLEDGMENTS

F. Randi and I. Vergara equally contributed to the present work. The authors are grateful to Daniel Khomskii for the insightful discussion and critical reading of the manuscript, and to Christian Schüßler-Langeheine for the discussion and the sample characterization. Research at the Università degli Studi di Trieste was supported by the Italian Ministry of Education, University and Research MIUR (SIR 2014, RBSI14ZIY2) and by the Friuli-Venezia Giulia region (European social fund, operative program 2007/2013). Research at Stanford was supported through the Stanford Institute for Materials and Energy Sciences (SIMES) under contract DE-AC02-76SF00515 by the US Department of Energy, Office of Basic Energy Sciences.

[1] E. J. W. Verwey, Nature (London) **144**, 327 (1939).
[2] D. I. Khomskii, *Transition Metal Compounds* (Cambridge University Press, Cambridge, UK, 2014).
[3] M. S. Senn, J. P. Wright, and J. P. Attfield, Nature (London) **481**, 173 (2012).
[4] E. Nazarenko, J. E. Lorenzo, Y. Joly, J. L. Hodeau, D. Mannix, and C. Marin, Phys. Rev. Lett. **97**, 056403 (2006).
[5] J. E. Lorenzo, C. Mazzoli, N. Jaouen, C. Detlefs, D. Mannix, S. Grenier, Y. Joly, and C. Marin, Phys. Rev. Lett. **101**, 226401 (2008).
[6] J. Garcia, G. Subías, J. Herrero-Martín, J. Blasco, V. Cuartero, M. C. Sánchez, C. Mazzoli, and F. Yakhou, Phys. Rev. Lett. **102**, 176405 (2009).
[7] S. C. Weng, Y. R. Lee, C. G. Chen, C. H. Chu, Y. L. Soo, and S. L. Chang, Phys. Rev. Lett. **108**, 146404 (2012).
[8] J. Blasco, J. Garcia, and G. Subias, Phys. Rev. B **83**, 104105 (2011).
[9] D. J. Huang, H. J. Lin, J. Okamoto, K. S. Chao, H. T. Jeng, G. Y. Guo, C. H. Hsu, C. M. Huang, D. C. Ling, W. B. Wu, C. S. Yang, and C. T. Chen, Phys. Rev. Lett. **96**, 096401 (2006).
[10] J. Schlappa, C. Schüßler-Langeheine, C. F. Chang, H. Ott, A. Tanaka, Z. Hu, M. W. Haverkort, E. Schierle, E. Weschke, G. Kaindl, and L. H. Tjeng, Phys. Rev. Lett. **100**, 026406 (2008).
[11] A. Tanaka, C. F. Chang, M. Buchholz, C. Trabant, E. Schierle, J. Schlappa, D. Schmitz, H. Ott, P. Metcalf, L. H. Tjeng,

and C. Schüßler-Langeheine, Phys. Rev. Lett. **108**, 227203 (2012).
[12] J. P. Wright, J. P. Attfield, and P. G. Radaelli, Phys. Rev. B **66**, 214422 (2002).
[13] Y. Fujii, G. Shirane, and Y. Yamada, Phys. Rev. B **11**, 2036 (1975).
[14] S. M. Shapiro, M. Iizumi, and G. Shirane, Phys. Rev. B **14**, 200 (1976).
[15] J. van den Brink and D. I. Khomskii, J. Phys. Condens. Matter **20**, 434217 (2008).
[16] J. P. Shepherd, J. W. Koenitzer, R. Aragón, C. J. Sandberg, and J. M. Honig, Phys. Rev. B **31**, 1107 (1985).
[17] S. de Jong, R. Kukreja, C. Trabant, N. Pontius, C. F. CHang, T. Kachel, M. Beye, F. Sorgenfrei, B. Back, C. H. Bräuer *et al.*, Nat. Mater. **12**, 882 (2013).
[18] A. Cavalleri, M. Rini, and R. W. Schoenlein, J. Phys. Soc. Jpn. **75**, 011004 (2006).
[19] M. Chollet, L. Guerin, N. Uchida, S. Fukaya, H. Shimoda, T. Ishikawa, K. Matsuda, T. Hasegawa, A. Ota, H. Yamochi, G. Saito, R. Tazaki, S. Adachi, and S. Koshihara, Science **307**, 86 (2005).
[20] D. Fausti, O. V. Misochko, and P. H. M. van Loosdrecht, Phys. Rev. B **80**, 161207 (2009).
[21] S. Borroni, E. Baldini, A. Mann, C. Arrel, F. van Mourik, J. Teyssier, J. Lorenzana, and F. Carbone, arXiv:1507.07193.
[22] A. Schlegel, S. F. Alvarado, and P. Wachter, J. Phys. C **12**, 1157 (1979).
[23] L. V. Gasparov, D. B. Tanner, D. B. Romero, H. Berger, G. Margaritondo, and L. Forrò, Phys. Rev. B **62**, 7939 (2000).
[24] S. K. Park, T. Ishikawa, and Y. Tokura, Phys. Rev. B **58**, 3717 (1998).
[25] I. Leonov, A. N. Yaresko, V. N. Antonov, and V. I. Anisimov, Phys. Rev. B **74**, 165117 (2006).
[26] K. J. Kim, S. Choi, H. J. Lee, J. H. Lee, and J. Y. Park, Solid State Comm. **143**, 285 (2007).
[27] F. Novelli, D. Fausti, J. Reul, F. Cilento, P. H. M. van Loosdrecht, A. A. Nugroho, T. T. M. Palstra, M. Grüninger, and F. Parmigiani, Phys. Rev. B **86**, 165135 (2012).
[28] F. Novelli, G. De Filippis, V. Cataudella, M. Esposito, I. Vergara, F. Cilento, E. Sindici, A. Amaricci, C. Giannetti, D. Prabhakaran *et al.*, Nat. Comm. **5**, 5112 (2014).
[29] A. J. M. Kuipers and V. A. M. Brabers, Phys. Rev. B **14**, 1401 (1976).
[30] A. Gössling, M. W. Haverkort, M. Benomar, H. Wu, D. Senff, T. Möller, M. Braden, J. A. Mydosh, and M. Grüninger, Phys. Rev. B **77**, 035109 (2008).
[31] A. Gössling, R. Schmitz, H. Roth, M. W. Haverkort, T. Lorenz, J. A. Mydosh, E. Müller-Hartmann, and M. Grüninger, Phys. Rev. B **78**, 075122 (2008).
[32] J. Reul, A. A. Nugroho, T. T. M. Palstra, and M. Grüninger, Phys. Rev. B **86**, 125128 (2012).
[33] See Supplemental Material at http://link.aps.org/supplemental/10.1103/PhysRevB.93.054305 for further details about the analysis of equilibrium and out-of-equilibrium data, about the calculation of the final effective temperatures, and for plots of the results at T = 80 and 140 K.
[34] Relevant with respect to noise.
[35] J. Reul, L. Fels, N. Qureshi, K. Shportko, M. Braden, and M. Grüninger, Phys. Rev. B **87**, 205142 (2013).
[36] R. V. Pisarev, A. S. Moskvin, A. M. Kalashnikova, and T. Rasing, Phys. Rev. B **79**, 235128 (2009).